Light Manipulation by Gold Nanobumps

Chia Min Chang · Cheng Hung Chu · Ming Lun Tseng ·
Yao-Wei Huang · Hsin Wei Huang · Bo Han Chen ·
Ding-Wei Huang · Din Ping Tsai

Abstract Backward and forward scattering of surface plasmonic wave interactions from gold nanobumps on the surface of a 30-nm gold thin film demonstrate three-dimensional (3-D) focusing and diverging properties. Fan-shaped forward scattering of an individual nanobump is observed. A quarter-circle structure composed of nanobumps is exploited to manipulate scattering from each nanobump. Experimental results show that 3-D propagation vectors generated by the gold nanobumps with their heights of 16 nm can deflect the surface plasmonic waves to produce 3-D focusing at 3.6 μm above the surface of the gold film. We clearly demonstrate that 3-D forward and backward focusing from gold nanobumps are with different amplitudes and directions of the vertical propagation vectors.

Introduction

Using plasmonic nanostructures to manipulate light is one of the important research and development topics of plasmonics [1]. Experiments demonstrated the manipulations of surface plasmon waves with chains of metal and dielectric nanoparticles fabricated on thin metallic films [2–7]. Several kinds of optical devices, such as a surface plasmon polariton mirror, beam splitter, and Mach–Zehnder interferometer, are developed in 2-D optics [8, 9]. The charming SPP subwavelength focusing and guiding properties are achieved by a quarter circular structure [10]. The bump structures are proposed to redirect and modify a surface plasmon wave [11], and the confined surface plasmon wave can be found in an elliptical corral [12]. The focusing and directing of surface plasmon waves by curved chains of nanoparticles were also theoretically investigated [13–17]. The dielectric material loaded on the metal surface can also focus and modulate the surface plasmon wave in 2-D optics [14–16]. Even the Huygens–Fresnel principle for surface plasmon wave diffraction, interference, and focusing was developed [17]. In addition, metallic nanoparticles are also of interest in applications including surface-enhanced Raman scattering [18, 19], plasmonic enhancement [20–24], and biological sensor [25]. In fact, the interactions between surface plasmon wave and nanostructure have three processes, including near-field reflection, transmission, and also far-field propagated light [26–29]. Most of the papers only reported the interactions in the

C. M. Chang · D.-W. Huang
Graduate Institute of Photonics and Optoelectronics,
National Taiwan University,
Taipei 106, Taiwan

C. M. Chang · C. H. Chu · H. W. Huang · B. H. Chen ·
D. P. Tsai (✉)
Department of Physics, National Taiwan University,
Taipei 106, Taiwan
e-mail: dptsai@phys.ntu.edu.tw

M. L. Tseng · Y.-W. Huang · D. P. Tsai
Graduate Institute of Applied Physics, National Taiwan University,
Taipei 106, Taiwan

D. P. Tsai
Research Center for Applied Sciences, Academia Sinica,
Taipei 115, Taiwan

D. P. Tsai
Instrument Technology Research Center, National Applied
Research Laboratories,
Hsinchu 300, Taiwan

near field and considered the far-field propagating light as a kind of loss. In fact, the far-field propagating light can be manipulated by nanostructures as well. In this letter, we experimentally investigate both the backward and forward scattering of surface plasmonic waves generated by the plasmonic nanostructures, such as gold (Au) nanobumps on an Au thin film. We would like to find out the focusing properties of Au nanobumps with each of their heights around 16 nm. Both focusing and diverging plasmonic nanostructures are fabricated on the same surface of the Au film to be imaged and studied simultaneously. Explicit scattering results of the Au nanobumps at the surface and out of the surface are shown.

Experimental

A Ti:sapphire femtosecond laser (Coherent Inc., γ=800 nm, pulse duration=140 fs, repetition rate=80 MHz) is used to fabricate the artificial structure as shown in Fig. 1a [30–32]. An attenuator and a shutter with switching time of 30 ms are used for the control of the incident laser fluence and exposure time. The laser beam is expanded to a diameter of 6 mm by a spatial filter. A γ/4 waveplate transforms the laser beam into circular polarization. Finally, the laser beam is focused by a high-numerical-aperture oil-immersion objective lens (Zeiss Plan-Apochromat, ×100, 1.4 NA, 0.17 mm working distance) through the transparent substrate on the 30-nm Au film on cover glass. An Au nanobump with its height around
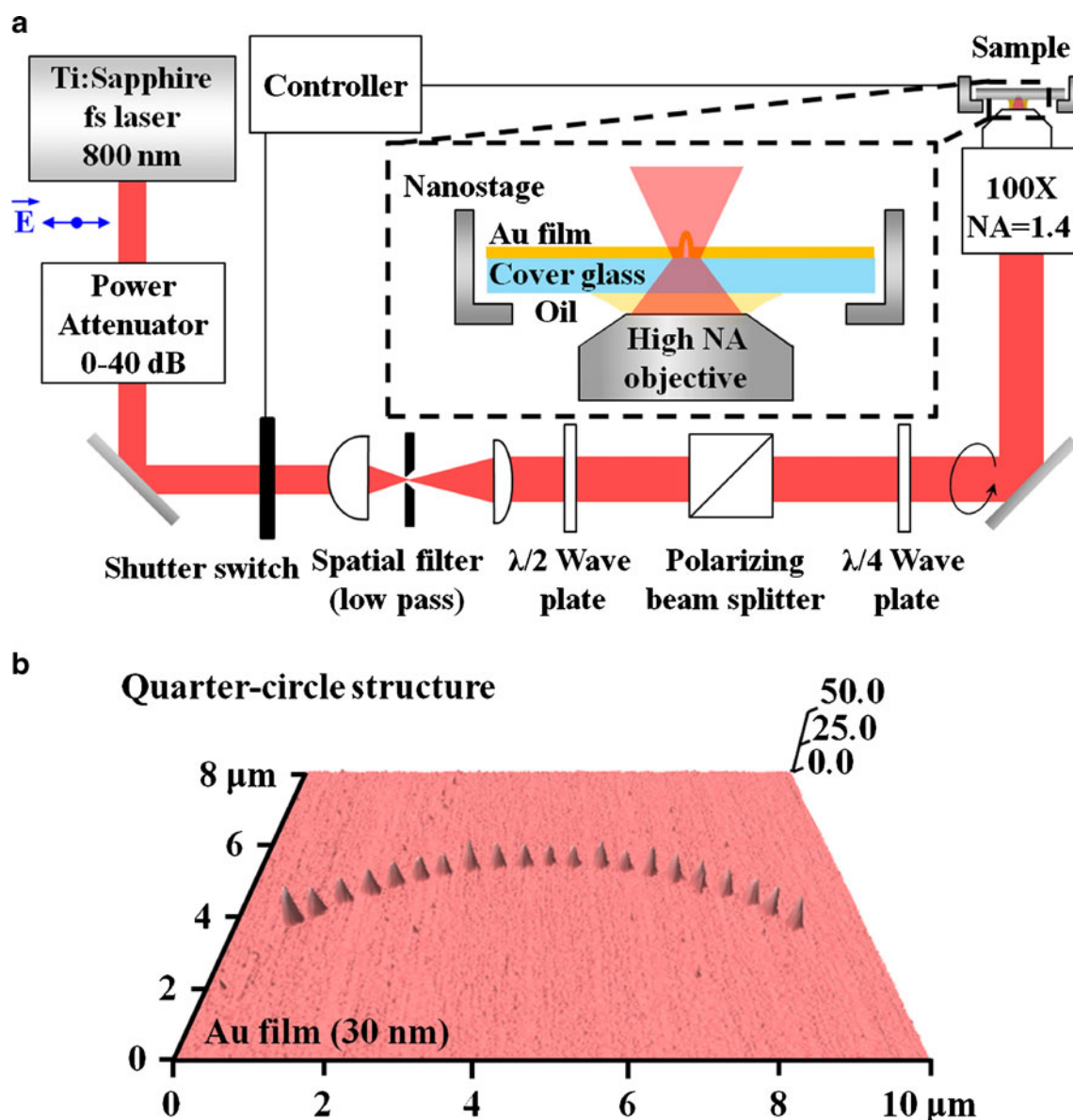

Fig. 1 a The schematic illustration of a femtosecond laser fabrication system. b 3-D AFM image of a quarter-circle structure formed by 21 nanobumps

16 nm can be fabricated with average laser power of 240 mW for 30 ms. The artificial plasmonic structure formed by nanobumps is made and controlled by a three-dimensional (3-D) nanometer precision stage (Mad City Lab. Inc., Nano-LP200). The surface morphology of the artificial structure is characterized by an atomic force microscope (AFM) (Asylum Research, MFP-3D). Figure 1b is 3-D AFM image of a quarter-circle structure composed of 21 nanobumps. The center-to-center distance of the nanobump is 450 nm. The average height and diameter of the base of the nanobump are around 16 and 300 nm, respectively.

The investigation of the light manipulation by the fabricated nanobumps is shown in Fig. 2. A total internal reflection microscope (TIRM) system based on an Olympus IX70 microscope and a Nd:YAG laser of 532 nm wavelength are used [33]. A fiber illuminator is built up to control the incidence angle of total internal reflection. An oil-immersion objective

(Olympus, Plan-Apo Oil TIRFM, ×60, N.A. 1.45) is used for this purpose. The polarization of the incident beam is set by the polarizer. The reflected laser beam is blocked by the stop, and the scattering light and dark field image can be captured by a CCD camera (Hamamatsu Co., ORCA-ER). We can adjust the focal plane of the objective along the z-axis to construct the trajectories of scattered light in 3-D. The inset shows that the surface plasmonic wave on the Au thin film is launched by a TM-polarized laser beam with an incident angle of 45°. Under this incident angle, the calculated surface plasmon wavelength, γ_{spp}, is 495.2 nm [34, 35]. The permittivity of the Au film used is $-4.4339+2.2618i$ [36, 37].

Results and Discussions

The topography and TIRM optical images of nanobumps are shown in Fig. 3. Figure 3a shows the 3-D AFM image of the
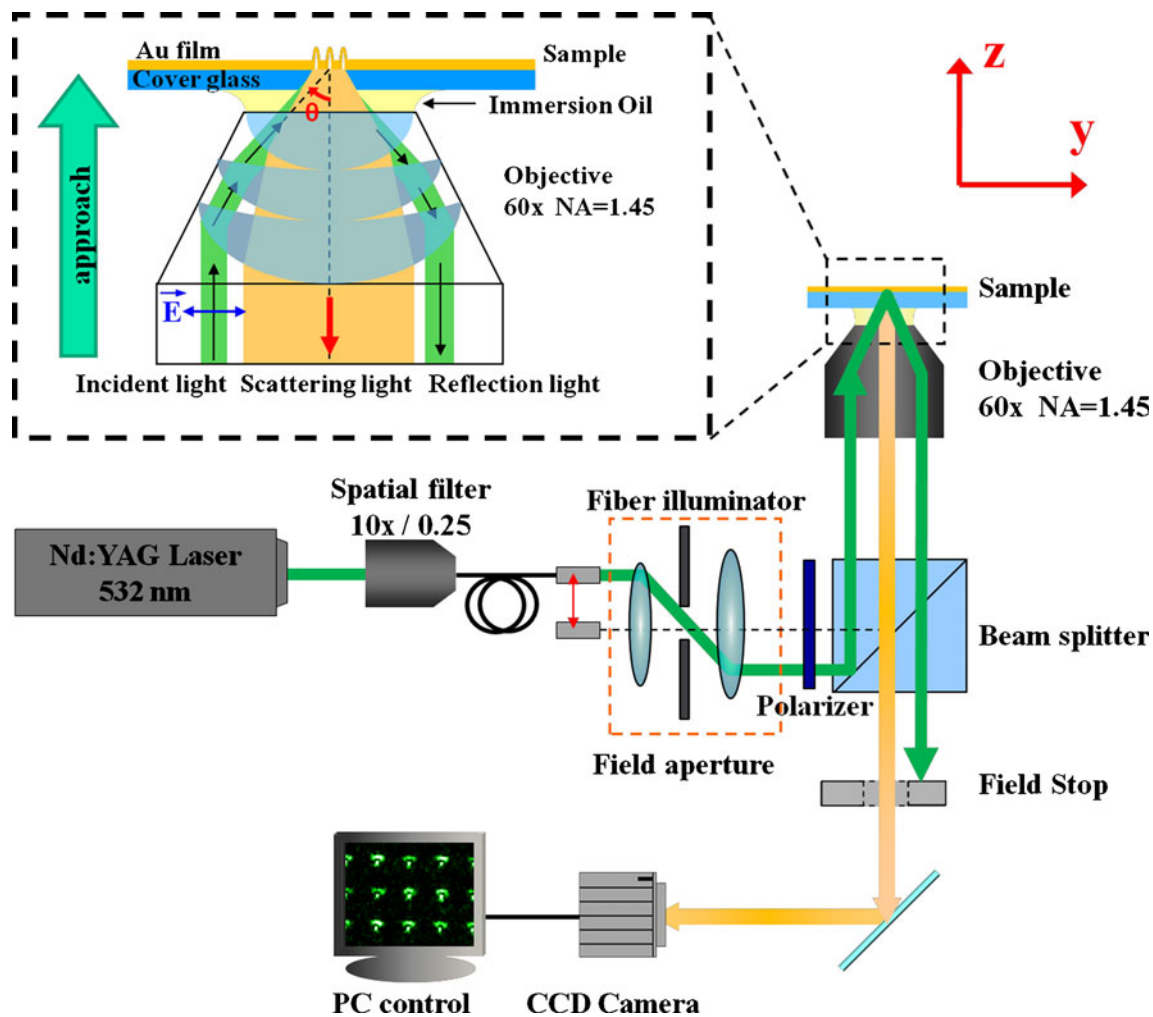

Fig. 2 The schematic of the total internal reflection microscope (TIRM) system for the investigation of the interactions of the laser-fabricated nanobumps. A high-numerical-aperture oil-immersed objective (×60, N.A. 1.45) is used to build up the surface plasmonic wave on the Au thin film and to collect the dark field image of the scattered light. The trajectories of scattered light can be captured and recorded by adjusting the focal plane along the z-axis

nanobump fabricated by a femtosecond laser on a 30-nm Au thin film. The coordinate axes are defined in the image, and the $z=0$ plane is set at the surface of the Au film. The period of nanobumps is 5 μm, and the height and the diameter of the base of each individual nanobump are 25 and 380 nm, respectively. The propagation direction of the surface plasmonic wave is along the y direction, which is marked by the green arrow. Impinging on nanobumps, the incoming surface plasmonic wave is scattered and imaged by the CCD camera. In Fig. 3b–f, we show frames of the acquired original video (media 1) of the area containing a 3×3 nanobump matrix at different z coordinates, and the images are captured form $-z$ to $+z$, respectively. Figure 3b is the image at $z=-2.77$ μm which shows the bright spots and patterns that were composed of both vertical $(-z)$ and backward $(-y)$ direction-scattering light of the surface plasmonic wave. Figure 3c shows that the image of the focal plane is at $z=-0.77$ μm, the intensity of the bright spots increased, and the pattern of the scattering light changed and converged. When the focal plane is at $z=0$, we found both backward and forward light-scattering patterns in Fig. 3d. At $z=0.73$ μm, bright spots and fan-shaped patterns are observed, as shown in Fig. 3e. The fan-shaped pattern separated at an angle around 105° clearly exhibits the forward-scattering light from the surface plasmonic wave. For the focal plane at $z=3.31$ μm, Fig. 3f shows the fan-shaped patterns extended further with less intensity, and the interference fringes can be seen. In general, TIRM images at different z

coordinates display the scattering light of the surface plasmon collected at that focal plane. The results of scattering light can be divided into two parts. At $z<0$, the bright spots and backward-scattering light are collected and shown, whereas the forward-scattering light can be observed at $z>0$. This provides us the opportunity of manipulation of the scattering light by creating specific patterns of the Au nanobumps.

For manipulation of the scattering light, the array of each quarter circle (90°) is designed and fabricated with 21 nanobumps. The 3-D AFM image of quarter-circle structures is shown in Fig. 4a, and the height and diameter of the base of each nanobump are around 16 and 300 nm, respectively. The distance of the adjacent nanobump is 450 nm. In the two columns of the left-hand-side of Fig. 4b–e, the structures are defined as "concave" relative to the propagation direction of the surface plasmon wave on the Au film. The structures in the two columns of the right-hand-side are then obviously regarded as "convex." Figure 4b shows the TIRM image which is captured under TE polarization illumination. Only a weak light pattern around concave and convex structures can be barely observed. Figure 4c–e shows the sequence TIRM images of the structures under TM polarization at different z coordinates. Figure 4c exhibits the image collected at $z=-3.8$ μm. The concave structures perform the function of focusing and successfully display bright focusing spots with two extended arms. On the contrary, the convex structures show the divergent fringes. An
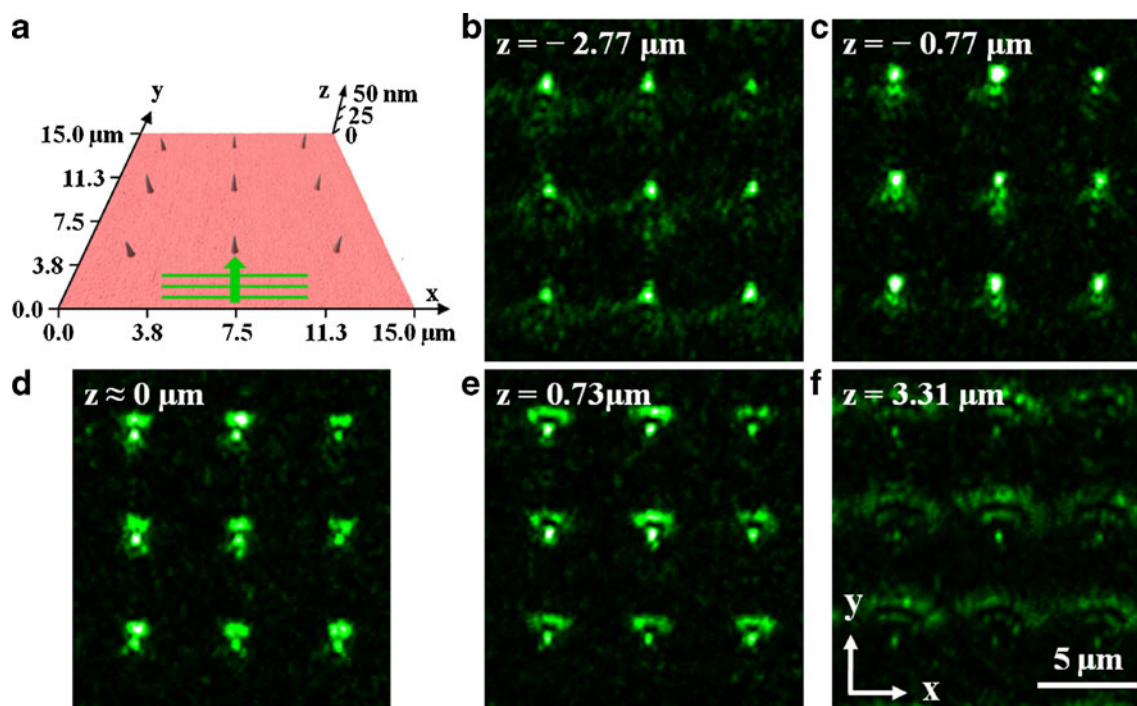

Fig. 3 **a** 3-D AFM image of a nanobump array with a 5-μm period on the Au thin film. The height and diameter of the base of the individual nanobump are 25 and 380 nm, respectively. Images **b** to **f** are the TIRM sequence images of nanobump array collected at different focal planes along the $+z$-axis (from negative to positive z) (media 1). The length of the *scale bar* is 5 μm
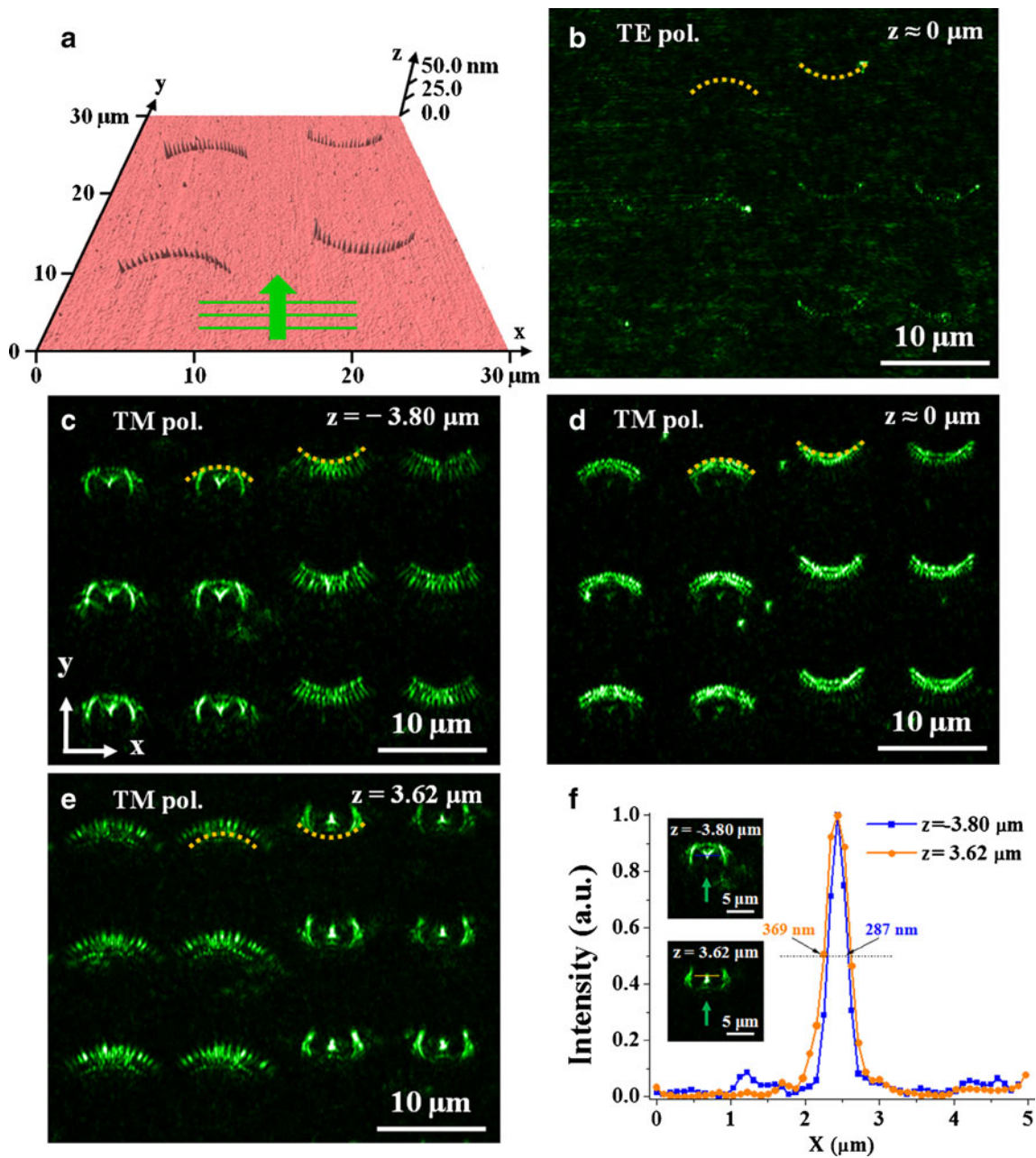
Fig. 4 a A 3-D AFM image of the quarter circles shows concave (*left*) and convex (*right*) structures composed of 21 nanobumps. The height of each nanobump is about 16 nm. **b–e** TIRM images of concave (*left two columns*) and convex (*right two columns*) quarter-circle structures. Image **b** is captured under TE polarization illumination. Images **c** and **d** are observed at various focal planes from $-z$ to $+z$ under TM polarization illumination (media 2). The input surface plasmon wave propagates in the $+y$ direction of the images. **f** The optical intensity profiles of the focusing spots of the concave and convex structure at $z=-3.8$ μm and $z=3.62$ μm, respectively

interesting thing is that they are all backward-scattering patterns. For the image collected near the Au thin film surface ($z\sim 0$ μm), Fig. 4d displays strong and bright patterns of the nanobumps and relatively weak focusing spots at the concave structures (left-hand-side columns). No focusing spots are shown in the convex structures. In Fig. 4e, at $z=3.62$ μm, the concave structures show divergent fringe patterns. A bright focusing spot with two extended arms can be seen at convex structures (right-hand-side columns). The

intensity profiles of the focusing spots at concave (Fig. 4c) and convex (Fig. 4e) structures are shown in Fig. 4f. The full-width-half-maximum of the intensity profiles are 287 and 369 nm for concave and convex structures shown in Fig. 4c and e, respectively. The change of image collected at the different focal plane is shown in media 2. We found the transformation of scattering light from focusing to diverging for concave structures, and it is reversed for the convex structures. Results demonstrate that we collect and observe

Fig. 5 Graphical description of the backward and forward scattering from the interactions between surface plasmon wave and nanobump
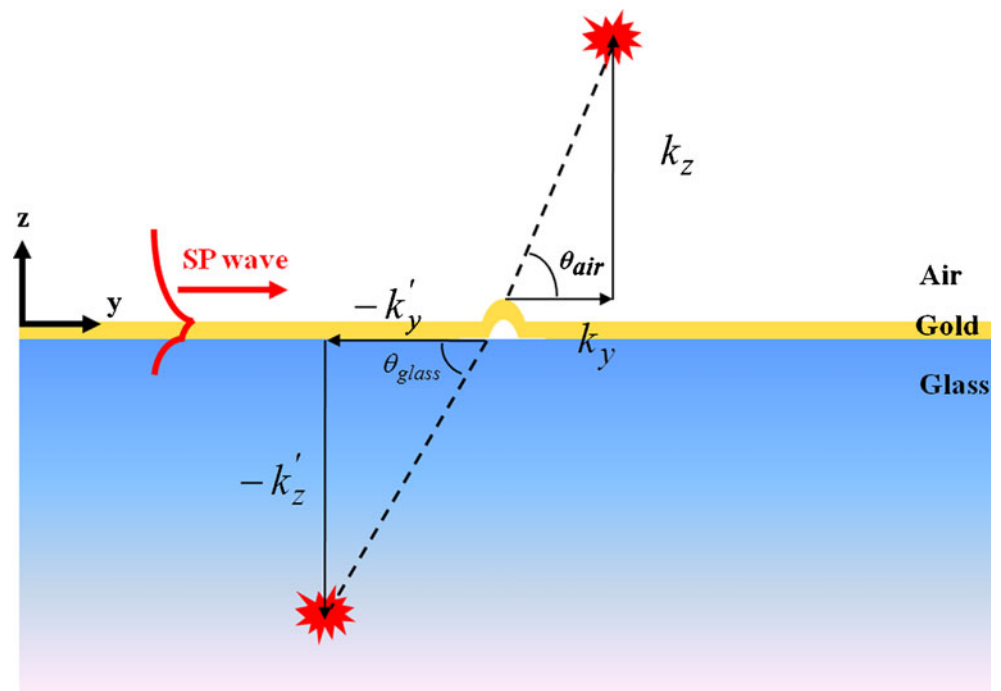
the backward scattering of the nanobumps either concave or convex structures at $z<0$. On the contrary, images of the forward-scattering light can be seen at $z>0$ only. For $z<0$, the projected patterns originate from the interference of the backward-scattering light of each nanobump. Concave structures clearly focus the backward-scattering light into an intense spot along with two interference arms; however, they can only show the divergent fringe patterns in the forward scattering. Convex structures show divergent fringe patterns in the backward-scattering conditions and confirm its focusing capability in the forward-scattering situations ($z>0$). Results evidently demonstrate that both concave and convex nanobump structures can strongly manipulate the surface plasmon wave at the surface of the Au film either backward or forward scattered away from the surface.

Figure 5 shows that the physics picture of the focusing spots is out of the Au surface due to the negative and positive propagating vectors ($-k_z$) and (k_z) generated by Au nanobumps in the vertical direction (z-axis). We found that nanobumps not only give backward and forward propagation vectors ($-k_x$, $-k_y$) and (k_x, k_y) for the manipulation of the light, but also provide negative and positive propagating vectors ($-k_z$) and (k_z) in the vertical direction (z-axis) for backward- and forward-scattering light, respectively. This is normally omitted or neglected in previous published papers. For the purpose of the plasmonic circuit applications at the surface of the plasmonic interface, most of the experimental results reported before showed the focusing of the surface plasmonic waves at the surface of the plasmonic waves. They neglected the possible propagating vectors ($-k_z$) and (k_z) generated in the vertical direction (z-axis) by the plasmonic nanostructures. However, our experimental results clearly demonstrated that propagating vectors generated in the vertical direction cannot be neglected for even an Au nanobump with its height less than 16 nm.

Conclusions

In summary, we have fabricated nanobumps on an Au thin film by using the femtosecond laser direct writing method and show that the surface plasmonic wave on the Au thin film can be scattered and manipulated by those Au nanobumps. Results clearly demonstrate the concave and convex nanobump structures can focus and diverge the surface plasmonic wave in backward-scattering direction, respectively. For the forward scattering, the concave and convex nanobump structure can diverge and focus the surface plasmonic wave, respectively. We found that focusing or diverging scattered light is not on the surface of the Au film. The Au nanobumps can generate 3-D propagation vectors ($-k_x$, $-k_y$, $-k_z$) and (k_x, k_y, k_z) for both backward and forward-scattering light, respectively. Our finding can provide great promise for versatile nanophotonics applications such as miniaturized optical data storage pick-up head focusing, plasmonic communication devices, and 3-D integrated photonic circuits, etc.

References

1. Bozhevolnyi SI, Volkov VS, Devaux E, Laluet JY, Ebbesen TW (2006) Channel plasmon subwavelength waveguide components including interferometers and ring resonators. Nature 440:508–511

2. Nomura W, Yatsui T, Ohtsu M (2006) Efficient optical near-field energy transfer along an Au nanodot coupler with size-dependent resonance. Appl Phys B 84:257–259

3. Radko IP, Bozhevolnyi SI, Evlyukhin AB, Boltasseva A (2007) Surface plasmon polariton beam focusing with parabolic nano-particle chains. Opt Express 15:6576–6582

4. Evlyukhin AB, Bozhevolnyi SI, Stepanov AL, Kiyan R, Reinhardt C, Passinger S, Chichkov BN (2007) Focusing and directing of surface plasmon polaritons by curved chains of nanoparticles. Opt Express 15:16667–16680

5. Kiyan R, Reinhardt C, Passinger S, Stepanov AL, Hohenau A, Krenn JR, Chichkov BN (2007) Rapid prototyping of optical components for surface plasmon polaritons. Opt Express 15:4205–4215

6. Radko IP, Bozhevolnyi SI, Brucoli G, Martin-Moreno L, Garcia-Vidal FJ, Boltasseva A (2009) Efficient unidirectional ridge excitation of surface plasmons. Opt Express 17:7228–7232

7. Zhang DG, Yuan XC, Bu J, Yuan GH, Wang Q, Lin J, Zhang XJ, Wang P, Ming H, Mei T (2009) Surface plasmon converging and diverging properties modulated by polymer refractive structures on metal films. Opt Express 17:11315–11320

8. Ditlbacher H, Krenn JR, Schider G, Leitner A, Aussenegg FR (2002) Two-dimensional optics with surface plasmon polaritons. Appl Phys Lett 81:1762–1764

9. Drezet A, Hohenau A, Stepanov AL, Ditlbacher H, Steinberger B, Aussenegg FR, Leitner A, Krenn JR (2006) Surface plasmon polariton Mach-Zehnder interferometer and oscillation fringes. Plasmonics 1:141–145

10. Yin LL, Vlasko-Vlasov VK, Pearson J, Hiller JM, Hua J, Welp U, Brown DE, Kimball CW (2005) Subwavelength focusing and guiding of surface plasmons. Nano Lett 5:1399–1402

11. Nomura W, Ohtsu M, Yatsui T (2005) Nanodot coupler with a surface plasmon polariton condenser for optical far/near-field conversion. Appl Phys Lett 86:181108

12. Drezet A, Stepanov AL, Ditlbacher H, Hohenau A, Steinberger B, Aussenegg FR, Leitner A, Krenn JR (2005) Surface plasmon propagation in an elliptical corral. Appl Phys Lett 86:3

13. Sterligov VA, Kretschmann M (2005) Scattering of surface electro-magnetic waves by Sn nanoparticles. Opt Express 13:4134–4140

14. Kim H, Hahn J, Lee B (2008) Focusing properties of surface plasmon polariton floating dielectric lenses. Opt Express 16:3049–3057

15. Wang Q, Yuan XC, Tan PS, Zhang DG (2008) Phase modulation of surface plasmon polaritons by surface relief dielectric structures. Opt Express 16:19271–19276

16. Fang ZY, Qi H, Wang C, Zhu X (2010) Hybrid plasmonic wave-guide based on tapered dielectric nanoribbon: excitation and focusing. Plasmonics 5:207–212

17. Teperik TV, Archambault A, Marquier F, Greffet JJ (2009) Huygens-Fresnel principle for surface plasmons. Opt Express 17:17483–17490

18. Lin WC, Liao LS, Chen H, Chang HC, Tsai DP, Chiang HP (2011) Size dependence of nanoparticle-SERS enhancement from silver film over nanosphere (AgFON) substrate. Plasmonics 6:201–206

19. Felidj N, Laurent G, Grand J, Aubard J, Levi G, Hohenau A, Aussenegg FR, Krenn JR (2006) Far-field Raman imaging of short-wavelength particle plasmons on gold nanorods. Plasmonics 1:35–39

20. Chen MW, Chau YF, Tsai DP (2008) Three-dimensional analysis of scattering field interactions and surface plasmon resonance in coupled silver nanospheres. Plasmonics 3:157–164

21. Chung HY, Leung PT, Tsai DP (2010) Enhanced intermolecular energy transfer in the vicinity of a plasmonic nanorice. Plasmonics 5:363–368

22. Yi M, Zhang D, Wen X, Fu Q, Wang P, Lu Y, Ming H (2011) Fluorescence enhancement caused by plasmonics coupling between silver nano-cubes and silver film. Plasmonics 6(2):213–217

23. Chau Y-F, Jiang Z-H (2011) Plasmonics effects of nanometal embedded in a dielectric substrate. Plasmonics 6(3):581–589

24. Chau Y-F, Chen MW, Yeh H-H, Wu F-L, Li H-Y, Tsai DP (2011) Highly enhanced surface plasmon resonance in a coupled silver nanodumbbell. Appl Phys A 104(3):801–805

25. Peng TC, Lin WC, Chen CW, Tsai DP, Chiang HP (2011) Enhanced sensitivity of surface plasmon resonance phase-interrogation biosensor by using silver nanoparticles. Plasmonics 6:29–34

26. Sanchez-Gil JA, Maradudin AA (1999) Near-field and far-field scattering of surface plasmon polaritons by one-dimensional surface defects. Phys Rev B 60:8359–8367

27. Shchegrov AV, Novikov IV, Maradudin AA (1997) Scattering of surface plasmon polaritons by a circularly symmetric surface defect. Phys Rev Lett 78:4269–4272

28. Zayats AV, Smolyaninov II, Maradudin AA (2005) Nano-optics of surface plasmon polaritons. Phys Rep 408:131–314

29. Kawazoe T, Yatsui T, Ohtsu M (2006) Nanophotonics using optical near fields. J Non-Cryst Solids 352:2492–2495

30. Chu CH, Chiun CD, Cheng HW, Tseng ML, Chiang HP, Mansuripur M, Tsai DP (2010) Laser-induced phase transitions of $Ge_2Sb_2Te_5$ thin films used in optical and electronic data storage and in thermal lithography. Opt Express 18:18383–18393

31. Chang CM, Chu CH, Tseng ML, Chiang HP, Mansuripur M, Tsai DP (2011) Local electrical characterization of laser-recorded phase-change marks on amorphous $Ge_2Sb_2Te_5$ thin films. Opt Express 19:9492–9504

32. Chu CH, Tseng ML, Shiue CD, Chen SW, Chiang HP, Mansuripur M, Tsai DP (2011) Fabrication of phase-change $Ge_2Sb_2Te_5$ nano-rings. Opt Express 19:12652–12657

33. Huang HJ, Yu CP, Chang HC, Chiu KP, Chen HM, Liu RS, Tsai DP (2007) Plasmonic optical properties of a single gold nano-rod. Opt Express 15(12):7132–7139

34. Chiu KP, Tsai DP (2005) Near-field interactions between light and surface plasmons of a metal slab. J Korean Phys Soc 47:S119–S122

35. Samson Z, Yen SC, Macdonald KF, Knight K, Li S, Hewak DW, Tsai DP, Zheludev NI (2010) Chalcogenide glasses in active plasmonics. Phys Status Solidi RRL 4:274

36. Chen WT, Wu PC, Chen CJ, Chung HY, Chau YF, Kuan CH, Tsai DP (2010) Electromagnetic energy vortex associated with sub-wavelength plasmonic Taiji marks. Opt Express 18:19665–19671

37. Chen WT, Chen CJ, Wu PC, Sun S, Zhou L, Guo GY, Hsiao CT, Yang KY, Zheludev NI, Tsai DP (2011) Optical magnetic response in three-dimensional metamaterial of upright plasmonic meta-molecules. Opt Express 19:12837–12842